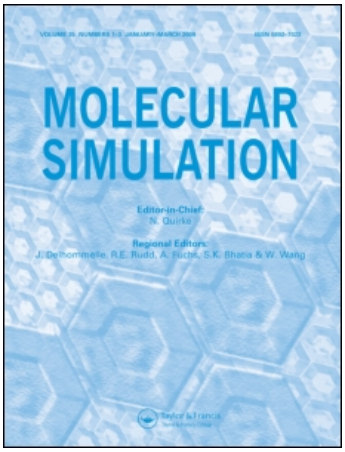

Molecular Simulation
Publication details, including instructions for authors and subscription information:
http://www.informaworld.com/smpp/title~content=t713644482

Docking and 3-D QSAR studies of dual PDE4-PDE7 inhibitors

N. S. Kang[a]; D. J. Jhon[a]; J. H. Song[a]; S. -E. Yoo[a]
[a] Korea Research Institute of Chemical Technology, Yusung-gu, Daejeon, South Korea

To cite this Article Kang, N. S. , Jhon, D. J. , Song, J. H. and Yoo, S. -E.(2007) 'Docking and 3-D QSAR studies of dual PDE4-PDE7 inhibitors', Molecular Simulation, 33: 14, 1109 — 1117
To link to this Article: DOI: 10.1080/08927020701630205
URL: http://dx.doi.org/10.1080/08927020701630205

Molecular Simulation, Vol. 33, No. 14, December 2007, 1109–1117

Taylor & Francis
Taylor & Francis Group

Docking and 3-D QSAR studies of dual PDE4-PDE7 inhibitors†

N. S. KANG*, D. J. JHON, J. H. SONG and S.-E. YOO

Korea Research Institute of Chemical Technology, P.O. Box 107, Yusung-gu, Daejeon 305-600, South Korea

(Received April 2007; in final form August 2007)

Small dual-specificity molecules inhibiting PDE4 and PDE7 can be used to treat inflammatory diseases. To design and synthesize dual PDE4 and PDE7 inhibitors, we carried out the target-based docking and the 3D QSAR study using CoMFA. Three compounds were synthesized. We predicted their inhibitory activities using our 3D QSAR model and tested their activities against PDE4 and PDE7 *in vitro*.

Keywords: Docking; PDE4; PDE7; 3D-QSAR; Inhibitor design

1. Introduction

Cyclic nucleotide phosphodiesterases (PDEs) [1,2] are enzymes that comprise 11 families. They hydrolyze the intracellular second messengers cyclic 3′,5′-adenosine and guanosine monophosphate (cAMP and cGMP) to AMP and GMP, respectively [3,4]. This type of hydrolysis is the only way to inactivate cAMP. Therefore, PDEs are important for regulating the cellular cyclic nucleotide concentrations. Three types of PDE occur: cAMP-specific (PDE4ABCD, PDE7AB and PDE8AB), cGMP-specific (PDE5A, PDE6ABC and PDE9A), and dual-specific (PDE1ABC, PDE2A, PDE3AB, PDE10A, and PDE11A) [5]. The cAMP-specific type 4 PDE (PDE4) [6,7] is an enzyme involved in the metabolism of cAMP in immune and inflammatory cells, such as eosinophils, T lymphocytes, macrophages, neutrophils, dendritic cells and epithelial cells. PDE4 inhibitors have been developed for treating chronic obstructive pulmonary disease (COPD) and asthma, including cilomilast (Ariflo) and roflumilast (Daxas) [8,9], which have reached the Phase III clinical trial stage. Unfortunately, these PDE4 inhibitors have a low therapeutic ratio because of their side effects, which include nausea, diarrhea, abdominal pain and vomiting [10]. To overcome the problem of side effects, studies are examining the development of mixed PDE inhibitors, including PDE4–PDE7 and PDE3–PDE4 inhibitors [11–13].

The cAMP-specific type 7 PDE (PDE7) is also restricted mainly to T cells and appears to play roles in asthma and COPD [14,15]. Two PDE7 genes (PDE7A and PDE7B) have been identified. PDE7A is expressed mainly in the lungs and immune system, whereas PDE7B is present in high concentrations in the pancreas, brain, heart, thyroid and skeletal muscle [16]. The enzymatic cores of PDE7B and PDE7A share approximately 70% homology.

Compounds that inhibit both PDE4 and PDE7 block the T cell component of disease and possess anti-inflammatory properties [11]. Such inhibitors should have fewer side effects, such as nausea and vomiting, and should act by maintaining high levels of intracellular cAMP. Therefore, to identify the structural features of dual PDE4–PDE7 inhibitors that can be used to design new inhibitors, we carried out molecular docking and 3D QSAR (CoMFA) studies of a series of 15 phthalazinone compounds and 11 well-known compounds. In addition, we synthesized three compounds and predicted their biological inhibition activities based on a model.

2. Computational details

2.1 Biological inhibition data and molecular structures

Table 1 shows the series of PDE4–PDE7 inhibitors studied. The initial structures of nine well-known

*Corresponding author. Tel.: + 82-42-860-7452. Fax: + 82-42-860-7635. Email: nskang@krict.re.kr

†The English in this document has been checked by at least two professional editors, both native speakers of English. For a certificate, see: http://www.textcheck.com/cgi-bin/certificate.cgi?id = qL4MDA

Molecular Simulation
ISSN 0892-7022 print/ISSN 1029-0435 online © 2007 Taylor & Francis
http://www.tandf.co.uk/journals
DOI: 10.1080/08927020701630205

Table 1. The compounds used in this study.

Code	Name	pIC_{50}[†]	pIC_{50}[‡]
01	(*cis*)-4-(3-chloro-4-methoxy-phenyl)-2-[1-(1-morpholin-4-yl-methanoyl)-piperidin-4-yl]-4a,5,8,8a-tetrahydro-2H-phthalazin-1-one	8.64	7.64
02	(*cis*)-4-(3-chloro-4-methoxy-phenyl)-2-[1-(toluene-4-sulfonyl)-piperidin-4-yl]-4a,5,8,8a-tetrahydro-2H-phthalazin-1-one	8.4	6.97
03	(*cis*)-2-(1-acetyl-piperidin-4-yl)-4-(3-chloro-4-methoxy-phenyl)-4a,5,8,8a-tetrahydro-2H-phthalazin-1-one	8.25	6.99
04	(*cis*)-4-(3-chloro-4-methoxy-phenyl)-2-(1-pyridin-4-ylmethyl-piperidin-4-yl)-4a,5,8,8a-tetrahydro-2H-phthalazin-1-one	8.61	7.38
05	(*cis*)-4-(3-chloro-4-methoxy-phenyl)-2-(4-{1-[4-(2-dimethylamino-ethyl)-piperidin-1-yl]-methanoyl}-phenyl)-4a,5,8,8a-tetrahydro-2H-phthalazin-1-one	7.86	7.18
06	(*cis*)-4-(3-chloro-4-methoxy-phenyl)-2-(6-methyl-3-trifluoromethyl-pyridin-2-yl)-4a,5,8,8a-tetrahydro-2H-phthalazin-1-one	7.64	7.08
07	(*cis*)-2-benzothiazol-6-yl-4-(3-chloro-4-methoxy-phenyl)-4a,5,8,8a-tetrahydro-2H-phthalazin-1-one	8.09	6.98
08	(*cis*)-4-(3-chloro-4-methoxy-phenyl)-2-(1-oxo-1,3-dihydro-isobenzofuran-5-yl)-4a,5,8,8a-tetrahydro-2H-phthalazin-1-one	8.05	7.05
09	(*cis*)-4-(3-chloro-4-methoxy-phenyl)-2-(1H-indazol-5-yl)-4a,5,8,8a-tetrahydro-2H-phthalazin-1-one	8.59	7.54
10	(*cis*)-4-(3-chloro-4-methoxy-phenyl)-2-cyclopentyl-4a,5,8,8a-tetrahydro-2H-phthalazin-1-one	9.11	7.73
11	(*cis*)-4-(3-chloro-4-methoxy-phenyl)-2-(4-imidazol-1-yl-butyl)-4a,5,8,8a-tetrahydro-2H-phthalazin-1-one	9.05	6.57
12	(*cis*)-4-{4-[4-(3-chloro-4-methoxy-phenyl)-1-oxo-4a,5,8,8a-tetrahydro-1H-phthalazin-2-yl]-butoxy}-benzoic acid	8.19	7.01
13	(*cis*)-4-[4-(3-fluoro-4-methoxy-phenyl)-1-oxo-4a,5,8,8a-tetrahydro-1H-phthalazin-2-yl]-benzoic acid	7.34	6.42
14	(*cis*)-4-(3-chloro-4-methoxy-phenyl)-2-(1,3,4-trimethyl-1H-pyrazolo[3,4-b]pyridine-6-yl)-4a,5,8,8a-tetrahydro-2H-phthalazin-1-one	7.66	7.38
15	(*cis*)-4-(3-chloro-4-methoxy-phenyl)-2-(3-thiophen-2-yl-[1,2,4]thiadiazol-5-yl)-4a,5,8,8a-tetrahydro-2H-phthalazin-1-one	7.63	7.11
16	2-[[4-[4-(dimethylamino)-1-piperidinyl]-6-[[(3,4,5-trimethoxyphenyl)methyl]amino]-2-pyrimidinyl]amino]-4-methyl-5-thiazolecarboxylic acid ethyl ester	5.52	7.52
17	2-[4,6-bis-(4-hydroxy-piperidin-1-yl)-pyrimidin-2-ylamino]-4-methyl-thiazole-5-carboxylic acid ethyl ester	5.49	7.22
18	Zardaverine[10]	6.41	3.7
19	Rolipram[10]	5.96	3.7
20	Filaminast[10]	6.0	6.0
21	Mesopram[10]	5.96	3.7
22	Cilomilast[10]	7.96	4.36
23	Roflumilast[10]	9.17	3.7
24	Piclamilast[10]	10.68	5.06
25	Sildenafil[10]	4.85	4.11
26	Vardenafil[10]	4.86	5.72

[†] The *in vitro* inhibitory activity against PDE4 enzyme; $pIC_{50} = -\log IC_{50(nM)}$; [‡] The *in vitro* inhibitory activity against PDE7 enzyme.

molecules (compounds 18–26 in table 1) obtained from ref. [17] were built based on their crystal structure. Models of the others were built using the structure of compound 10 and minimized using the CHARMM32b1 force field. Their biological inhibition data were obtained from patent documents [18,19].

The 3D structure of PDE4 was taken from the Brookhaven Protein Databank (PDB code 1PTW). PDE7 shares approximately 32% homology with PDE4. The sequence of the 321 residues of PDE7 was taken from the SwissProt database (www.expasy.org/uniprot/Q13946). To build the 3D structure of PDE7, we used the automated protein homology-modeling server SWISS-MODEL [20], and molecular dynamics simulation techniques using the CHARMM32b1 force field in an explicit solvent model with a distance-dependent dielectric constant [21]. The conformations of the active sites of PDE4 and PDE7 built from their crystal structures and homology modeling are compared in figure 1. Table 2 compares the active site residues of PDE4 and PDE7.

Three new compounds were synthesized using the route shown in schemes 1 and 2 in Appendix.

2.2 Molecular docking and 3D QSAR studies

Nine molecules obtained from X-ray crystallography studies were minimized using the CHARMM32b1 force field with a distance-dependent dielectric constant and the steepest descent minimization algorithm. Various trials were carried out to obtain credible binding models for the 17 molecules for which the binding model was unknown. We chose the best model that showed a good correlation between the binding energies and biological inhibitory activities of the compounds, and then we used the chosen model as the basis for alignment in 3D QSAR studies. We used a sp^3 carbon atom and a + 1 net charge atom as a steric and electronic field energy probe for the 3D QSAR

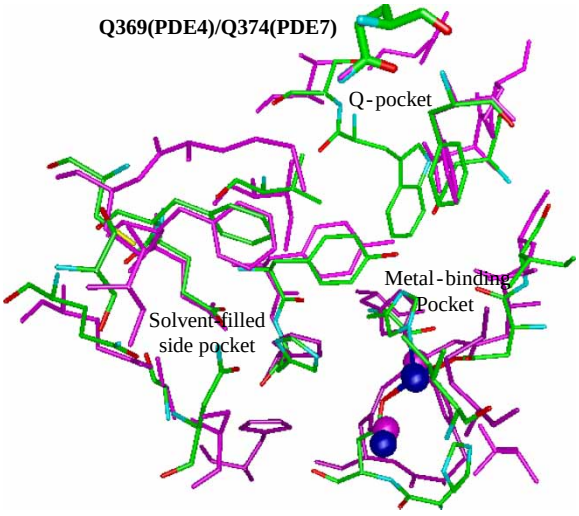

Figure 1. The comparison between the conformation of PDE7-PDE4 active sites (Element color: PDE7, magenta: PDE4). Also the pockets described in table 2 are shown. Two blue (or magenta) balls are metal atoms like zinc. The above residues shown as thick stick are Q369 (PDE4) and Q374 (PDE7) known as catalytic residue (colour in online version).

Table 2. A comparison of the active site residues of PDE4 and PDE7.

Function	*Symbol*	*PDE4*	*PDE7*
Metal-binding pocket	M	H160, H164, H200, D102, H204, N209, L229, E230, D272, M273, D318	H173, H177, H213, D214, H217, Q222, L242, E243, D283, I284, D323
Q-pocket	Q	Y159, L319, N321, P322, Y329, W332, T333, I336, M337, M357, V365, S368, Q369, F372	Y172, I324, N326, P327, S334, W337, S338, V341, C342, L362, I370, I373, Q374, F377
Solvent-filled side pocket	S	G206, S208, E339, F340, Q343, S355, C358	G219, N221, E344, F345, Q348, S360, C363

studies. A Tripos force field with a distance-dependent dielectric constant at all interactions in a regularly spaced (2 Å) grid was used for the steric and electronic interactions. The energy cutoff was set to 30 kcal/mol, and a regression analysis was performed using the full cross-validated partial least squares (PLS) method of leave-one-out with the CoMFA standard options for scaling variables. The minimum sigma was set to 2.0 kcal/mol to improve the signal-to-noise ratio by omitting those lattice points whose energy variation was below this threshold. The final model obtained from the non-cross-validated conventional analysis was developed with the optimal number of components equal to that with the highest q^2. All the molecular modeling calculations were conducted using version 7.1 of the program SYBYL on a Linux system.

3. Results and discussion

Figure 2 shows the credible binding conformational alignment of the 17 compounds for which the binding model was not known. Based on this binding model, we

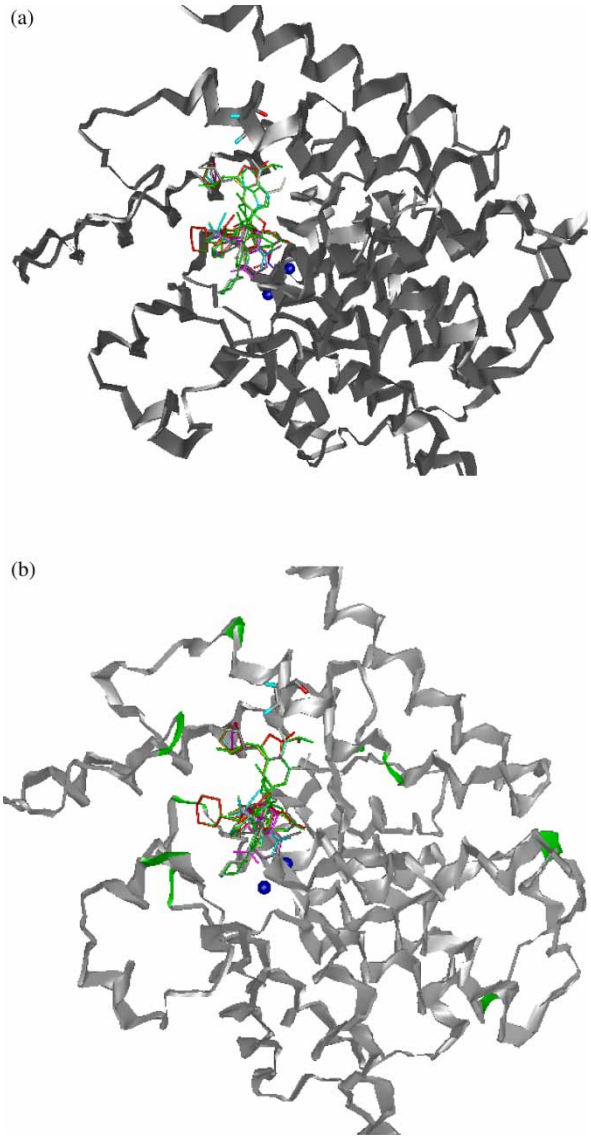

Figure 2. The binding alignment of 17 inhibitors for which the binding model was not known against (a) PDE4 (b) PDE7.

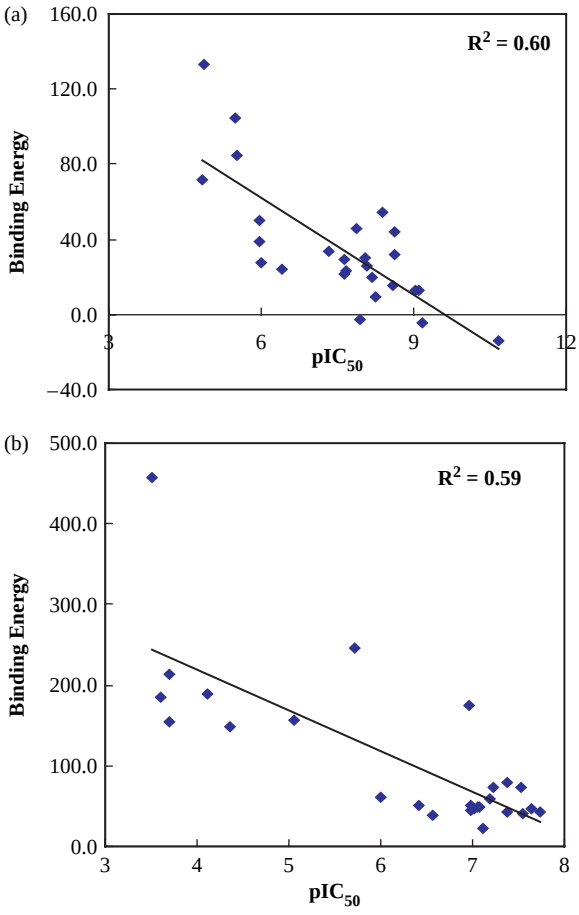

Figure 3. The binding energy correlation plot for (a) PDE4 and (b) PDE7. (The binding energy is represented by kcal/mol).

calculated the binding energies for each compound from the CHARMM force field [21]. We show the correlation between the binding energies and biological inhibitory activities in figure 3. The correlation coefficients for PDE 4 and PDE 7 were 0.60 and 0.59, respectively, demonstrating that our binding conformations and the binding models of the compounds used were reasonable and reliable. Figure 4 show the binding models of docked inhibitors 18–21 with PDE4 and PDE7. These results reproduced the known crystallized conformations of these compounds [17].

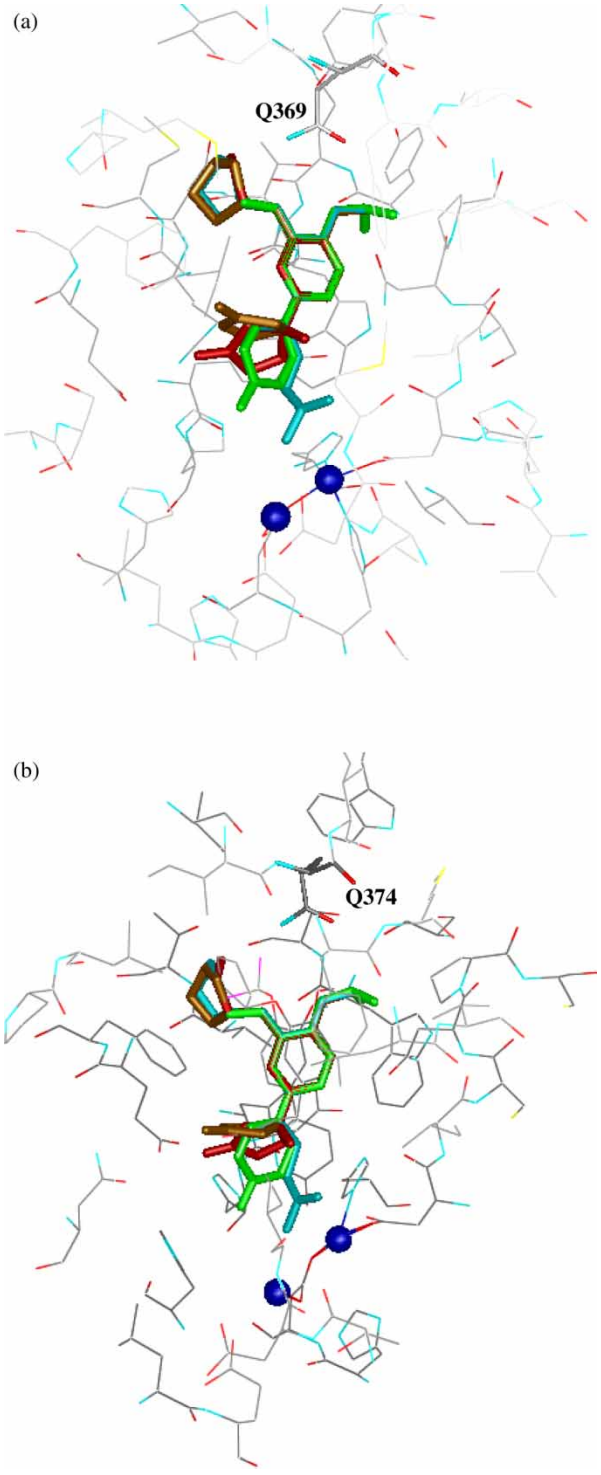

Figure 4. The complex structure of (a) PDE4 and (b) PDE7 with compounds 18 (green), 19 (brown), 20 (cyan) and 21 (red) (colour in online version).

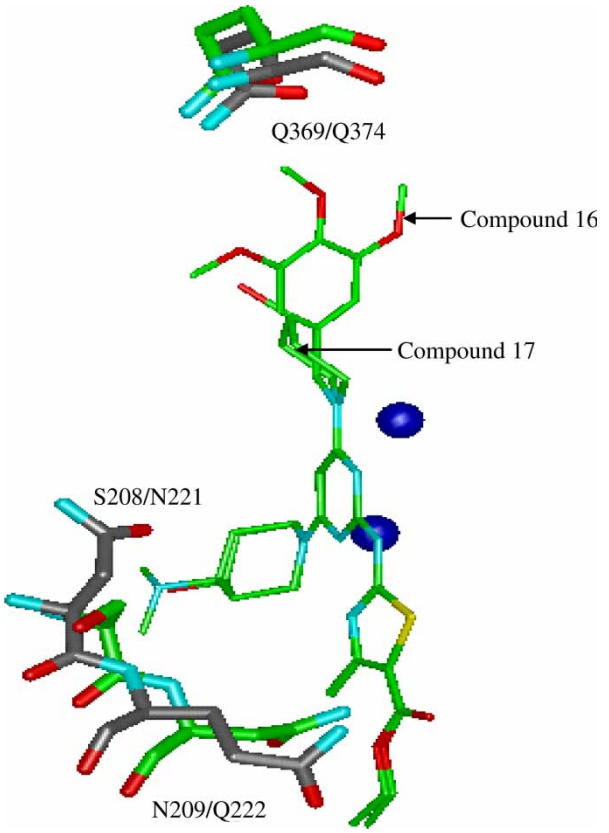

Figure 5. Comparison of the binding mode with PDE4/PDE7 for compounds 16 and 17.

We focused on inhibitors 16 and 17, which showed a poor interaction with PDE4, but a good interaction with PDE7. As shown in figure 5 and table 2, the side chains N209/Q222 at the metal-binding site and S208/N221 at the solvent-filling side pocket of PDE4/PDE7 were positioned differently. The direction and conformation of Q222 and N221 of PDE7 were more favorable in the interactions with inhibitors 16 and 17.

We performed a PLS analysis of the PDE4 and PDE7 inhibitors, and the results are shown in table 3. The predicted activities of a real external testing set, consisting of the three compounds synthesized, are shown in table 4.

Table 3. The CoMFA results for PDE4 and PDE7 inhibitors.

		Cross-validated		*Non-cross validated*		
		$q^{2\dagger}$	$N^{\ddagger}$	$r^{2\P}$	$S^{\S}$	$F^{\|\|}$
CoMFA	PDE4	0.64	4	0.98	0.26	185.83
	PDE7	0.68	3	0.96	0.33	138.89

† Cross-validated correlation coefficient; ‡ The number of components; ¶ Conventional correlation coefficient; § Standard error of estimate; || *F*-test values.

Table 4. The observed and predicted activities of the three synthesized compounds used in the test set.

Test set[†]	*PDE-4$_{obs}$*[‡]	*PDE-4$_{pred}$*[‡]	*PDE-7$_{obs}$*[‡]	*PDE-7$_{pred}$*[‡]
Com01	7.22	7.09	4.22	4.53
Com02	7.30	7.08	4.53	4.60
Com03	6.37	7.80	4.80	4.99

[†] The three compounds in the test set are shown below. [‡] "obs" indicates the inhibitory activities obtained experimentally and "pred" denotes the value predicted from the CoMFA model.

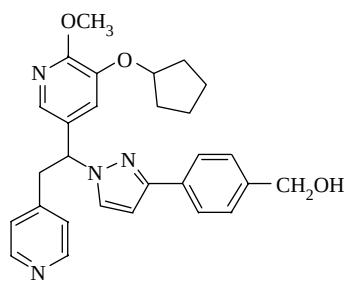

Com01

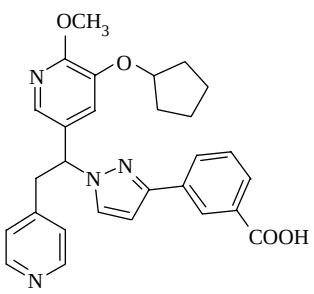

Com02

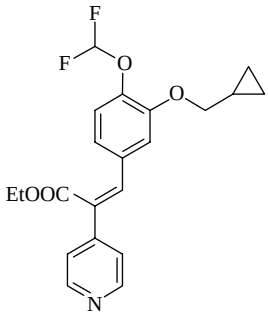

Com03

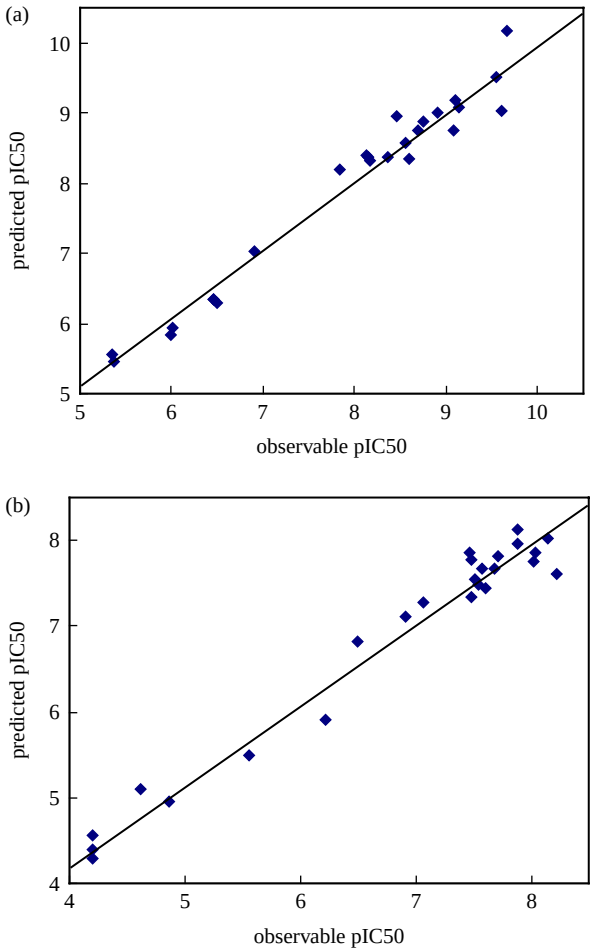

Figure 6. The correlation plots of the predicted activities (predicted pIC_{50}) versus the experimental activities (observable pIC_{50}) for (a) PDE4 (b) PDE7.

The correlation plots of the predicted activities (predicted pIC_{50}) versus their experimental activities (observed pIC_{50}) are depicted in figure 6 for PDE4 and PDE7. Table 3 and figure 6 demonstrate that the activities predicted by the CoMFA model are in good agreement with the experimental data. Thus, the CoMFA model constructed based on the docking model is reliable.

Figure 7 shows 3D coefficient contour interaction maps of the CoMFA results for PDE4 in (a) and PDE7 in (b). The CoMFA contour map is mapped with the PDE4 and PDE7 active sites in figure 8. This demonstrates regional variation in the steric and electrostatic characteristics of the structural features for the different molecules contained in the training set that increases or decreases the biological activity. In these contour maps, the green regions indicate areas where a sterically bulkier group enhances the enzymatic inhibitory activity, while the yellow regions show that a sterically less bulky group favors the inhibitory activity. Blue regions suggest areas where more positively charged groups favor the enzymatic inhibitory activity, while red regions indicate that more negatively charged groups favor this activity.

The CoMFA contour map showed favorable regions for the steric interaction, indicated as the green contour around the metal-binding pocket and solvent-filled side pocket in PDE4 and PDE7. In comparison to the CoMFA map between PDE4 and PDE7, the steric-related CoMFA map of the region around the Q-pocket showed that PDE7 admitted bulkier substitutes than PDE4. This is why the I336 residue in the Q-pocket of PDE4 corresponds to the V341 residue in the Q-pocket of PDE7. Notably, substitutes near the Q-pocket in PDE7 allow a less bulky group than those in PDE4; this occurs because the S368 residue in the Q-pocket of PDE4 changes to an I274 residue in the Q-pocket of PDE7, and the side chain of the I274 residue extends into part of the Q-pocket as shown in table 2. The region between the metal-binding pocket and

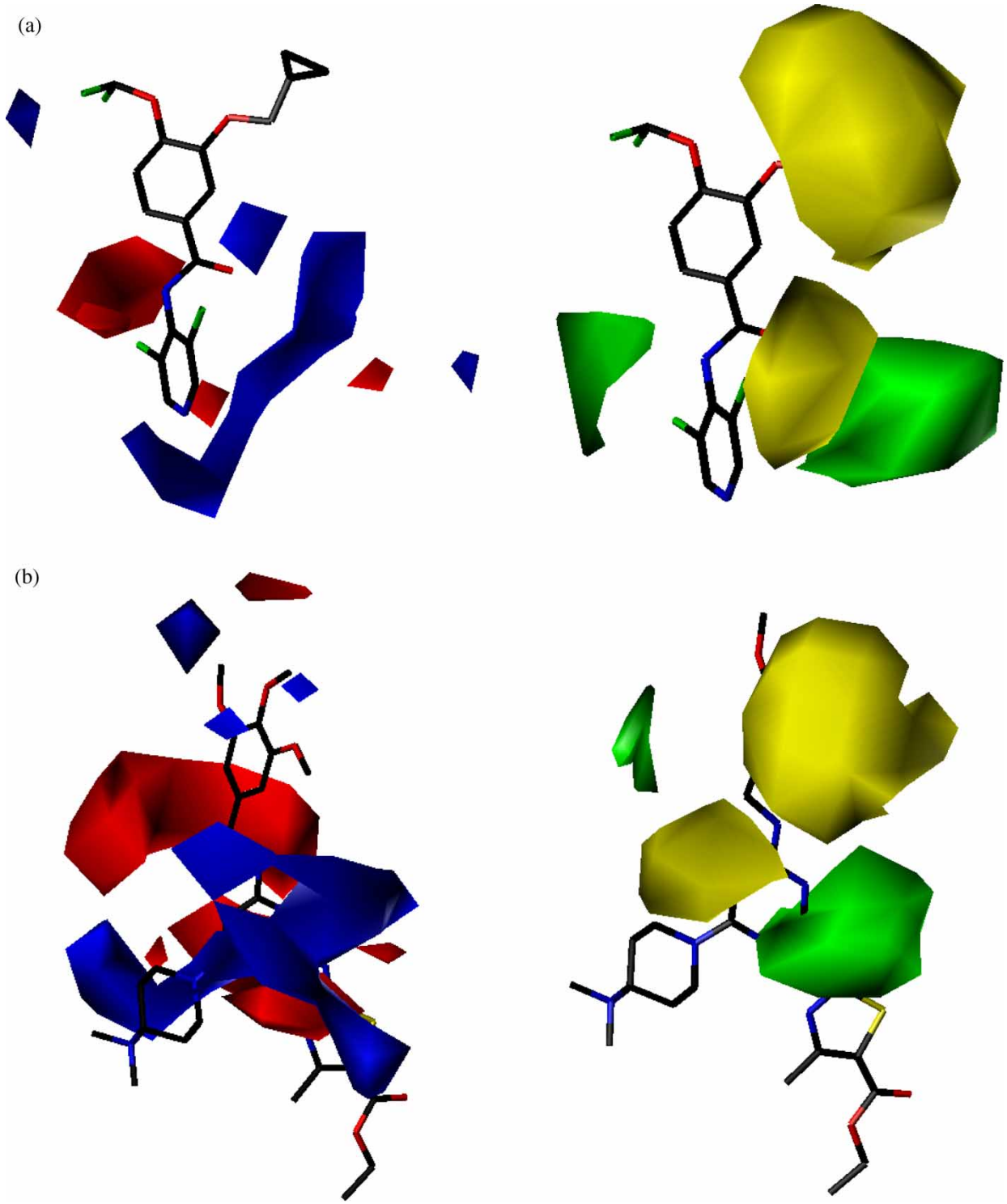

Figure 7. The CoMFA interaction contour maps are shown (a) for PDE4 and (b) for PDE7. In these contour maps, the green regions indicate areas where a sterically bulkier group enhances the enzymatic inhibitory activity, while the yellow regions show that a sterically less bulky group favors the inhibitory activity. Blue regions suggest areas where more positively charged groups favor the enzymatic inhibitory activity, while red regions indicate that more negatively charged groups favor this activity (colour in online version).

solvent-filled side pocket is yellow in PDE4 only. In this region, the side chain of the M274 residue in PDE4 is flexible and thus can adopt two stable conformations as shown in figure 9. But for our training set, the side chain of M274 residue adopts the conformation like as 1OYN in figure 9, so restricts the small approaching compounds. In addition, the region between the Q-pocket and metal-binding pocket showed that PDE4 allows larger groups to enhance the activity compared to PDE7. In several reported PDE4 complex structures, a water molecule is

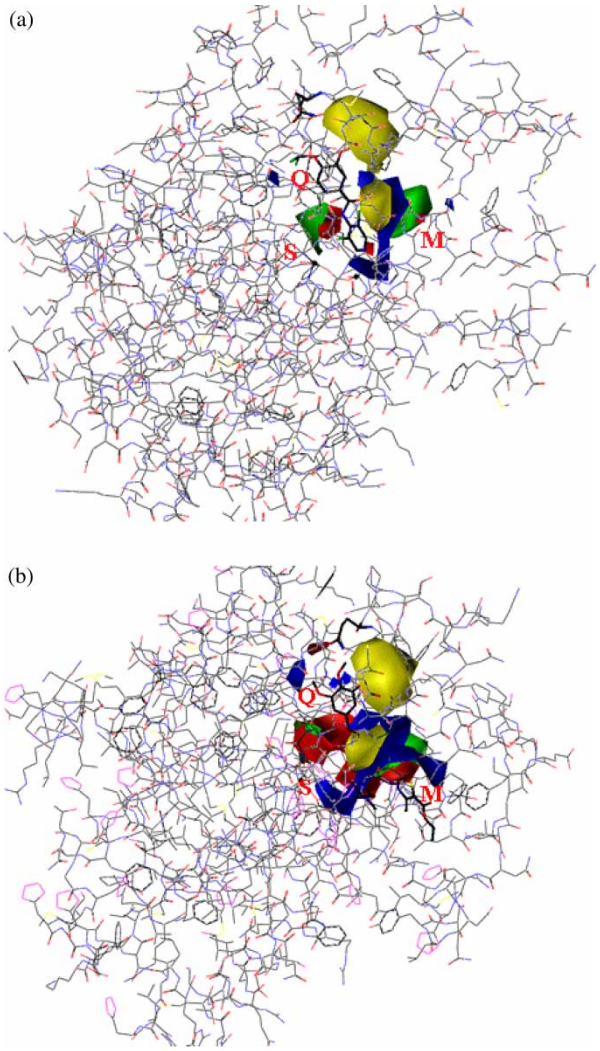

Figure 8. The Mapping of CoMFA contour map with (a) PDE4 (b) PDE7 active sites. Q, S and M represent Q-pocket, solvent-filled side pocket and metal-binding pocket, respectively.

found in this region [17,22–24]. Therefore, substitutes near the metal-binding region might allow some bulky and electronegative groups, as shown in figure 7(a). In the metal-binding region, both PDE4 and PDE7 prefer to accept an electronegative substitute that interacts with metal ions via an indirect water-bridged hydrogen bond [25,26], such as a pyridine or pyridine oxide. Particularly in PDE7, more red is seen in the map near the metal-binding region due to the N221 residue in the solvent-filled side pocket and the Q222 in the metal-binding pocket. Based on these results, we considered the interaction with the Q-pocket and solvent-filled side pocket in designing dual PDE4 and PDE7 inhibitors and synthesized the three compounds shown in table 4 and schemes 1 and 2.

As a reference compound, we used roflumilast ($pIC_{50} = 9.17$, $pIC_{50} = 3.7$ for PDE4 and PDE7) [17], which has reached Phase III status. The 1-(cyclopropylmethoxy)-2-difluoromethoxy benzene moiety of roflumilast, with a volume of 668.82, was changed to a 3-(cyclopentyloxy)-2-methoxypyridine having a volume of 642.36 to reduce the

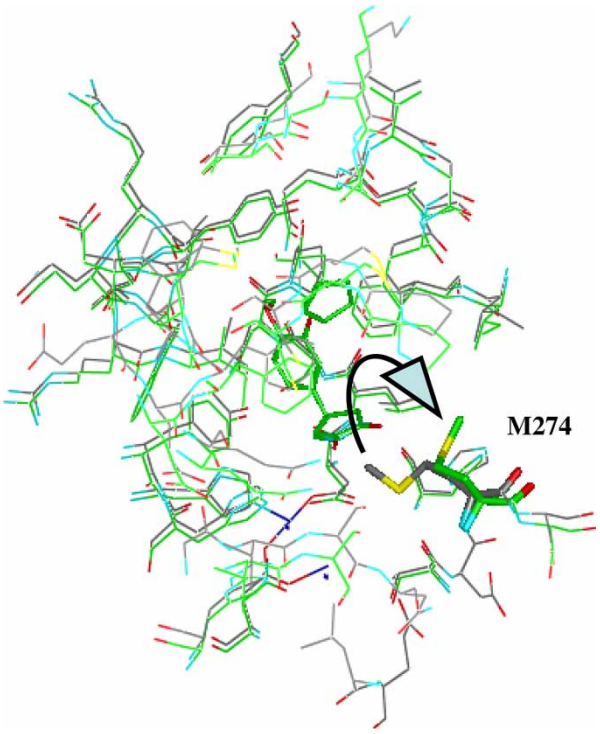

Figure 9. The side chain flexibility of M274 residue found in the crystallized structure of Protein data bank (1TBB[24] in gray element color and 1OYN[10] in green element color) (colour in online version).

volume of the moiety in the Q-pocket slightly. In addition, to compensate for the interaction with the solvent-filled side pocket, we introduced a pyrazole moiety and its derivatives, as shown in table 4. These compounds (Com01; $pIC_{50} = 4.22$, Com02: $pIC_{50} = 4.53$) were nearly eight times more potent than roflumilast at inhibiting PDE7 *in vitro*, while their activities against PDE4 were not enhanced. Conversely, retaining the roflumilast moiety that interacts with the Q-pocket, while changing the moiety interacting with the solvent-filled side pocket and Q-pocket, we synthesized compound Com03, which has a carboxyethyl group. Com03 showed improved inhibition, and its activity against PDE7 was ten times greater than that of roflumilast *in vitro*, while the inhibition of PDE4 decreased to 43 nM ($pIC_{50} = 6.37$).

In conclusion, this observation combining 3D QSAR and a binding study led to the design and synthesis of dual PDE4 and PDE7 inhibitors. Further studies will optimize these compounds with dual PDE4 and PDE7 inhibitory activities for treating inflammatory disease, asthma, and COPD.

Acknowledgements

This research was supported by a grant (CBM31-B2000-01-00-00) from the Center for Biological Modulators of the 21st Century Frontier R&D Program, the Ministry of Science and Technology, Korea

Appendix

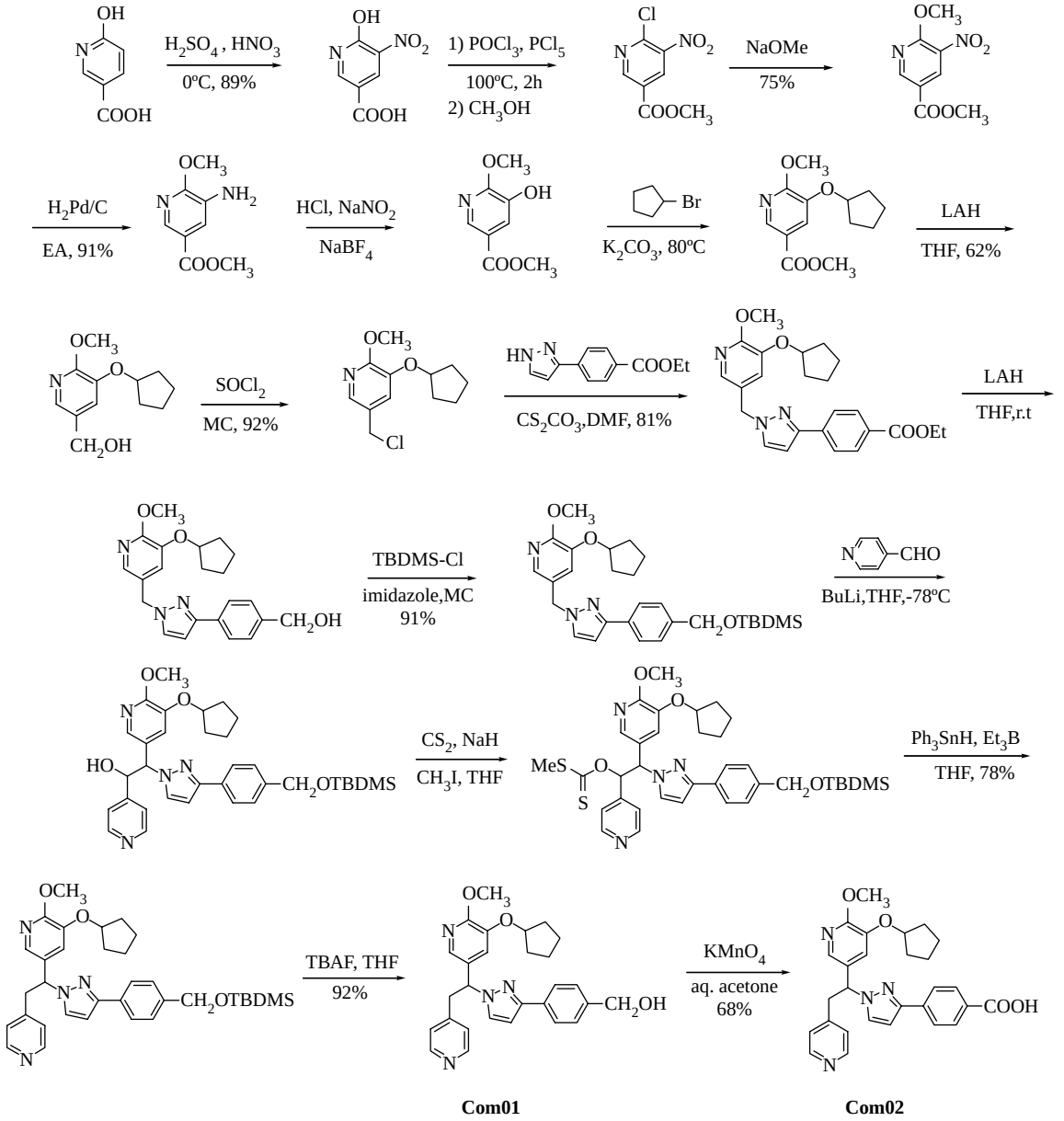

Scheme 1.

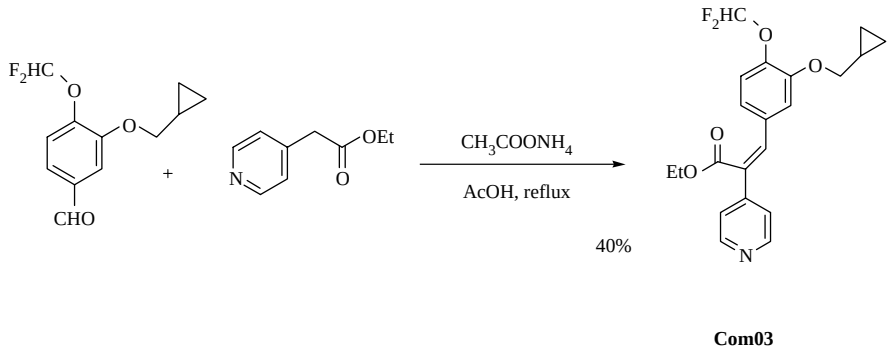

Scheme 2. We prepared **com 1** starting from 6-hydroxynicotinic acid in 17 steps with an overall yield of 3%. **Com 3** was obtained by the condensation of 3-Cyclopropylmethoxy-4-difluoromethoxybenzaldehyde and pyridin-4-yl-acetic acid ethyl ester using ammonium acetate in 40% yield.

References

[1] J.A. Beavo. Cyclic neclotide phosphodiesterases; functional implications of multiple isoforms. *Physiol. Rev.*, **75**, 725 (1995).

[2] M. Conti. Phosphodiesterases and cyclic nucleotide signaling in endocrine cells. *Mol. Endocrinol.*, **14**, 1317 (2000).

[3] C. Mehats, C.B. Anderson, M. Filopani, S.L. Jin, M. Conti. Cyclic necleotide phosphodiesterases and their role in endocrine cell signaling. *Trends Endocrinol. Metab.*, **13**, 29 (2002).

[4] S.H. Francis, I.V. Turko, J.D. Corbin. Cyclic nucleotide phosphodiesterases: relating structure and function. *Prog. Nucleic Acid Res. Mol. Biol.*, **65**, 1 (2001).

[5] J.A. Beavo, L.L. Brunton. Cyclic nucleotide research-still expanding after half a century. *Nat. Rev. Mol. Cell Biol.*, **3**, 710 (2002).

[6] M.S. Barnette, J.O. Bartus, M. Burman, S.B. Cheistensen, L.B. Cieslinski, K.M. Esser, U.S. Prabhakar, J.A. Rush, T.J. Torphy. Association of the anti-inflammatory activity of phos-phodiesterase 4 (PDE4) inhibitors with either inhibition of PDE4 catalytic activity or competition for [^{3}H]rolipram binding. *Biochem. Pharm.*, **51**, 949 (1996).

[7] M.D. Houslay, D.R. Adams. PDE4 cAMP phosphodiesterases: modular enzymes that orchestrate signaling cross-talk, desensitization and compartmentalization. *Biochem. J.*, **370**, 1 (2003).

[8] M.S. Barnette, S.B. Christensen, D.M. Eaasyan, M. Grous, U. Prabhakar, J.A. Rush, A. Kagey-Sobotka, T.J. Torphy. SB 207499 (Ariflo), a potent and selective second-generation phosphodiesterase 4 inhibitor: *in vitro* anti-inflammatory actions. *J. Pharmacol. Exp. Ther.*, **284**, 420 (1998).

[9] A. Hatzelmann, C.J. Schudt. Anti-inflammatory and immunomodulatory potential of the novel PDE4 inhibitor roflumilast *in vitro*. *J. Pharmacol. Exp. Ther.*, **297**, 267 (2001).

[10] A. Robichaud, P.B. Stamatiou, S.L. Jin, N. Lachance, D. MacDonald, F. Laliberte, S. Liu, Z. Huang, M. Conti, C.C. Chan. Deletion of phosphodiesterase 4D in mice shortens alpha(2)-adrenoreceptor-mediated anesthesia, a behavioral correlate of emesis. *J. Clin. Invest.*, **110**, 1045 (2002).

[11] M.A. Giembycz. Life after PDE4: overcoming adverse events with dual-specificity phosphodiesterase inhibitors. *Curr. Opin. Pharmacol.*, **238**, 5 (2005).

[12] T.J. Torphy, B.J. Undem, L.B. Cieslinski, M.A. Luttman, M.L. Reeves, D.W. Hay. Identification, characterization and functional role of phosphodiesterases isozymes in human airway smooth muscle. *J. Pharmacol. Exp. Ther.*, **265**, 1213 (1993).

[13] G. Yang, K.W. Mclntyre, R.M. Townsend, H.H. Shen, W.J. Pitts, J.H. Dodd, S.G. Nadler, M. McKinnon, A.J. Watson. Phosphodiesterase 7A-deficient mice have functional T cells. *J. Immnunol.*, **171**, 6414 (2003).

[14] S.J. Smith, S. Brookes-Fazakerley, L.E. Donnelly, P.J. Barnes, M.S. Bernette, M.A. Giembycz. Ubiquitous expression of phosphodiesterase 7A in human pro-inflammatory and immune cells. *Am. J. Physiol.*, **284**, L279 (2003).

[15] C. Gardner, N. Robas, D. Cawkill, M. Fidock. Cloning and characterization of the human and mouse PDE7B, a novel cAMP-specific cyclic nucleotide phosphodiesterase. *Biochem. Biophys. Res. Commun.*, **272**, 186 (2000).

[16] J.M. Hetman, S.H. Sodering, N.A. Glavas, J.A. Beavo. Cloning and characterization of PDE7B, a cAMP-specific phosphodiesterase. *Proc. Natl. Acad. Sci. USA*, **97**, 472 (2000).

[17] G.L. Card, B.P. England, Y. Suzuki, D. Fong, B. Powell, B.H. Lee, C. Luu, M. Tabrizizad, S. Gillette, P.N. Ibrahim, D.R. Artis, G. Bollag, M.V. Milburn, S.H. Kim, J. Schlessinger, Y.J. Zhanh. Structural basis for the activity of drugs that inhibit phosphodiesterases. *Structure*, **12**, 2233 (2004).

[18] A. Hatzelmann, D. Marx, W. Steinhilber, A.G. Altana Pharma. Phthalazinone derivatives useful as PDE4/7 inhibitors. World Patent WO02085906 (2002).

[19] W.J. Pitts, A.J. Watson, J.H. Dodd. Bristol-Myers Squibb. Dual inhibitors of PDE7 and PDE4. World Patent WO02088079 (2002).

[20] T. Schwede, J. Kopp, N. Guex, M.C. Peitsch. SWISS-MODEL: an automated protein homology-modeling server. *Nucleic Acids Res.*, **31**, 3381 (2003).

[21] B.R. Brooks, R.E. Bruccoleri, B.D. Olafson, D.J. States, S. Swaminathan, M. Karplus. CHARMM: a program for macromolecular energy, minimization, and dynamics calculations. *J. Comp. Chem.*, **4**, 187 (1983).

[22] R. Terry, Y.F. Cheung, M. Praetegaard, G.S. Baillie, E. Huston, I. Gall, D.R. Adams, M.D. Houslay. Occupancy of the catalytic site of the PDE4A4 cyclic AMP phosphodiesterase by rolipram triggers the dynamic redistribution of this specific isoform in living cells through a cyclic AMP independent process. *Cell. Signal.*, **15**, 955 (2003).

[23] R.X. Xu, A.M. Hassell, D. Vanderwall, M.H. Lambert, W.D. Holmes, M.A. Luther, W.J. Rocque, M.V. Milburn, Y. Zhao, H. Ke, R.T. Nolte. Atomic structure of PDE4: insights into phosphodiesterase mechanism and specificity. *Science*, **288**, 1822 (2000).

[24] K.Y.J. Zhang, G.L. Card, Y. Suzuki, D.R. Artis, D. Fong, S. Gillette, D. Hsieh, J. Neiman, B.L. West, C. Zhang, M.V. Milburn, S.H. Kim, J. Schlessinger, G. Bollag. A glutamine switch mechanism: short article for nucleotide selectivity by phosphodiesterases. *Mol. Cell*, **15**, 279 (2004).

[25] N.S. Kang, D.H. Jung, K.T. No, M.S. Jhon. Molecular dynamics simulation of Na^+-DMP^- and Na^+-MP^{2-} ion pair in aqueous solution. *Chem. Phys. Lett.*, **364**, 580 (2002).

[26] N.S. Kang, C.H. Chae, S.E. Yoo. Study on the hydrolysis mechanism of phosphodiesterase 4 using molecular dynamics simulations. *Mol. Sim.*, **32**, 369 (2006).